

The Compact Structure of Radio-Loud Broad Absorption Line Quasars

Y. Liu^{1,3*}, D. R. Jiang^{1,3}, T. G. Wang^{2,3}, F. G. Xie^{1,3,4}

¹ *Shanghai Astronomical Observatory, Chinese Academy of Sciences, Shanghai 200030, China.*

² *Center for Astrophysics, University of Science and Technology of China, Hefei, Anhui 230026, China*

³ *Joint Institute for Galaxy and Cosmology (JOINGC) of SHAO and USTC*

⁴ *Graduate School of Chinese Academy of Sciences, Beijing 100039, China*

5 November 2018

ABSTRACT

We present the results of EVN+MERLIN VLBI polarization observations of 8 Broad Absorption Line (BAL) quasars at 1.6 GHz, including 4 LoBALs and 4 HiBALs with either steep or flat spectra on VLA scales. Only one steep-spectrum source, J1122+3124, shows two-sided structure on the scale of 2 kpc. The other four steep-spectrum sources and three flat-spectrum sources display either an unresolved image or a core-jet structure on scales of less than three hundred parsecs. In all cases the marginally resolved core is the dominant radio component. Linear polarization in the cores has been detected in the range of a few to 10 percent. Polarization, together with high brightness temperatures (from $2 \times 10^9 - 5 \times 10^{10}$ K), suggest a synchrotron origin for the radio emission. There is no apparent difference in the radio morphologies or polarization between low-ionization and high-ionization BAL QSOs nor between flat- and steep-spectrum sources. We discuss the orientation of BAL QSOs with both flat and steep spectra, and consider a possible evolutionary scenario for BAL QSOs. In this scenario, BAL QSOs are probably the young population of radio sources, which are Compact Steep Spectrum or GHz peaked radio source analog at the low end of radio power.

Key words: galaxies: active – galaxies: jets – quasars: absorption lines – quasars: general

* E-mail: yliu@shao.ac.cn

1 INTRODUCTION

About 10 - 20% of optically selected quasars exhibit Broad Absorption Line (BAL) troughs up to $\sim 0.1c$ blueward of their corresponding emission lines (Weymann et al. 1991; Weymann 2002; Tolea et al. 2002; Hewett & Foltz 2003; Reichard et al. 2003). These BALs are produced via resonant scattering in partially ionized outflows. BAL quasars can be further divided into high- and low-ionization sub-classes (HiBALs and LoBALs). HiBAL quasars are those objects which show BALs only in highly ionized species such as CIV and NV, while LoBAL quasars also show BALs in Mg II or Al III. Two different scenarios have been proposed to explain the BAL phenomena. In the first scenario, the BAL region (BALR) is present with a small covering factor in every QSO. The different appearance of BAL and non-BAL QSOs is solely due to different lines of sight. In a BAL QSO our line of sight intercepts the BALR while it does not in non-BAL QSOs. In this scenario, the fraction of BAL QSOs is interpreted as the covering factor of BALRs. This paradigm has also been generalized to interpret the dichotomy of LoBAL and HiBAL as an orientation effect, in which low-ionization outflow covers small fraction sky with the BAL outflow. This scenario is consistent with a number of statistical properties, such as the similarity between the UV continuum and emission line spectra for both types of QSOs (e.g., Weymann et al. 1991), their similar millimeter and far-infrared luminosities (e.g., Willott et al. 2003), as well as their similar large scale environments (Shen et al. 2008). In the second scenario BALs exist only in a relative short phase of QSO activity, which is very likely in their early phase of evolution, at least for LoBAL QSOs (Briggs, Turnshek & Wolfe 1984). Support for the latter scenario includes the excess fraction of LoBAL quasars among infrared selected quasars (Boroson & Meyers 1992), and a special locus in black hole mass versus accretion rate space (Boroson 2002).

In the first scenario the BALR is probably located in a preferred direction with respect to the system's symmetry axis, e.g., in the equatorial or polar direction. Higher polarization in the optical continuum in comparison to non-BAL QSOs suggests that BAL QSOs are seen nearly edge-on (Goodrich & Miller 1995; Hines & Wills 1995; Cohen et al. 1995; Wang, Wang & Wang 2005). Equatorial outflows are also preferred from theoretical considerations for radiatively accelerated winds from an accretion disc or evaporated gas from a putative dusty torus (Punsly 2006).

However, there are indications for both polar and equatorial outflows in radio-loud BAL QSOs. It is generally believed that the radio jet is aligned with the symmetry axis of the

accretion disk. Thus it can be taken as an indicator of the system inclination. According to the unification scheme of radio quasars, a radio-loud quasar would show a flat radio spectrum and a core-dominated morphology when viewed along the radio jet, due to relativistic boosting of the optically thick core. It would appear as a steep-spectrum radio source with double-lobed morphology when viewed side-ways (e.g., Urry & Padovani 1995). Thus the radio morphology and spectrum can serve as a surrogate for the inclination of the system: in an equatorial outflow model a radio-loud BAL QSO would appear as a steep-spectrum radio source with double-lobed radio morphology, while the opposite situation will be observed in a polar-outflow model. Becker et al. (2000) found that BAL QSOs in the FIRST Bright Quasar Survey (FBQS) display both steep and flat radio spectra (see also Menou et al. 2001), indicating both polar and equatorial outflows. Other studies suggest a similar result. On the one hand, nearly a dozen double-lobed FR II quasars were found, mostly from the SDSS and FIRST samples (Wills, Brandt, & Loar 1999; Gregg et al. 2000; Brotherton et al. 2002; Zhou et al. 2006; Gregg, Becker & de Vries 2006). On the other hand, evidence for polar outflows has also been found in a small number of radio variable BAL QSOs (Zhou et al 2006; Ghosh & Punshly 2007), in which the radio variability suggests that the radio jet is beamed towards the observer. The presence of both polar and equatorial outflows can be better interpreted in the context of an evolutionary scenario, rather than the geometrical unification scheme.

Further studies of radio-loud BAL QSOs are necessary in order to fully understand the geometry of outflows in their population. Note that most radio-loud BAL QSOs with steep radio spectra show compact structures on VLA scales, different from classical radio-loud quasars on which the unification scheme is based. Thus it is not clear whether the radio spectrum can be used as an indicator for inclination or not. Powerful FR II radio BAL QSOs are extremely rare among radio-loud BAL QSOs, and most radio BAL QSOs are only moderately strong in the radio. Morphological studies of these radio intermediate BAL quasars can reveal representative properties of the majority radio population of BAL QSOs. Currently, less than a handful of such BAL QSOs have been studied at sufficiently high angular resolution and they have revealed a complex situation.

In previous EVN observations, Jiang & Wang (2003) observed 3 BAL quasars at L band using the phase reference technique. Among these three sources, only one (J1312+2319) has compact two-sided structure, and the other two are still unresolved. The jet orientation might

be near the line of sight if the compact component is the jet base in these two unresolved sources. In this case the orientation model may be problematic, at least for these 3 sources.

In this paper, we report our EVN+MERLIN observations at 1.6 GHz of eight BAL quasars, including equal numbers of HiBAL and LoBAL quasars and then give some discussion of the results. § 2 presents the observations as well as data reduction and the results are described in § 3. The discussion is contained in § 4, and in the last section § 5 we give the conclusions. Throughout the paper we adopt the spectral index convention $f_\nu \propto \nu^{-\alpha}$ and a cosmology with $H_0 = 70 \text{ km s}^{-1} \text{ Mpc}^{-1}$, $\Omega_M = 0.3$, $\Omega_\Lambda = 0.7$. All values of luminosity used in this paper are calculated with our adopted cosmological parameters.

2 OBSERVATION AND DATA REDUCTION

Our BAL quasars are comparatively bright sources ($\sim 10 \text{ mJy}$), which have been selected from the Becker et al. (2000) BAL quasar sample. EVN+MERLIN phase-reference polarimetric continuum observations were made for 8 BAL quasars at L band on 2005 June 22. The observations were divided into two runs, each lasting 12 hours. In order to compare the radio morphology of either low- and high-ionization or steep- and flat-spectrum BAL quasars, our sample included 4 LoBAL quasars and 4 HiBAL quasars with both steep and flat spectra on VLA scales. The left/right-circular polarization signals were recorded in 8 baseband channels with a total bandwidth of 32 MHz and 2-bit sampling. The angular distances of the phase referencing sources to the target sources are less than 3° . The scan time for each source was about 1.5 hours, and the estimated thermal noise in the total intensity images was no more than 0.1 mJy/beam . We used OQ208/J1407+284 and J0927+3902 as the D-term calibrators for the 1st and 2nd runs, respectively, and 3C286/J1331+305 as the electric vector polarization angle (EVPA) calibrator for both runs. The EVN data were correlated at the Joint Institute for VLBI in European (JIVE) in Dwingeloo. Pipeline results were used for the phase referencing. Since the flux densities of all BAL quasars in our sample except J1603+3002 are lower than 20 mJy on VLA scales, we used non-phase referencing results of J1603+3002 (about 54 mJy , which is strong enough to detect with normal fringe fitting) to compare with the results from phase referencing. The results are in good agreement, suggesting that the phase referencing observations of the other sources should also be reliable. The initial amplitude calibration and the fringe-fitting were performed using the NRAO Astronomical Image Processing System (AIPS). The imaging and self-calibration

Table 1. Sources observed with EVN+MERLIN at 18 cm. The source name (in J2000) and GST range are shown in Column(1) and Column(2). The VLA spectral index and VLA flux density at 20 cm are listed in Column(3) and Column(4), while the EVN and MERLIN flux density at 18 cm are shown in Column(5) and Column(6) respectively. The last Column is the classification of BAL quasars.

Name(s)	GST range (Europe)	α ($S_\nu \propto \nu^\alpha$)	VLA (mJy at 20 cm)	EVN (mJy at 18 cm)	MERLIN (mJy at 18 cm)	Note
J0724 + 4159	22:00-14:00	0.0	7.9 (B)	7.2	8.0	LoBAL
J0728 + 4026	22:00-14:00	-1.1	18.0 (A)	16.1	17.6	LoBAL
J1044 + 3656	02:00-18:00	-0.5	15.6 (A)	16.4	18.5	LoBAL
J1122 + 3124	03:00-17:00	-0.6	12.9 (B)	8.3	10.2	LoBAL
J1150 + 2819	04:00-17:00	-1.2	14.2 (B)	12.6	12.3	HiBAL
J1413 + 4212	05:00-21:00	-0.2	18.7 (B)	17.1	18.1	HiBAL
J1603 + 3002	08:00-21:00	-0.6	54.2 (A)	52.1	52.6	HiBAL
J1655 + 3945	08:00-23:00	-0.2	10.2 (A)	12.1	10.6	HiBAL

Note: GST range is unique, eliminate reference to Europe.

were carried out in the DIFMAP package (Shepherd, Pearson, & Taylor 1994) and these self-calibrations allowed us to improve the signal to noise ratio in the images. The estimated uncertainty of the amplitude calibration is about 10 percent. The detailed information for these observations are listed in Table 1 and Table 2, including total flux densities from both EVN and MERLIN, positions shifts, fractional polarization, EVPA as well as uncertainty for polarization. Moreover, making use of the phase-reference technique, we were able to obtain positions from the VLBI data which are more accurate than those obtained from the VLA. Table 3 lists all the position information for target BAL sources and phase-reference sources. The position of the phase tracking center for BAL sources is shown in column (2) and column (3), while the name and position of the phase-reference sources are denoted in column (4), column (5) and column (6), respectively. In our sample, J1044+3656 has the largest shift away from its phase tracking center, about 225 mas east and 225 mas south. Although these shifts might affect the signal to noise ratio, the EVN flux densities of our sources are similar to those observed at the VLA, suggesting that their influence is too small to be important. The accurate positions of the BAL quasars calculated from the shifts away from the phase tracking centers are listed in the last two columns in Table 3. The 3σ uncertainty in these positions, which mainly depends on both the angular resolution of the EVN at 18 cm and the signal to noise ratio, is ~ 15 mas.

Table 2. EVN+MERLIN observational details of BAL quasars at 18 cm.

Sources Name	Position EVN (mas)	Position MERLIN (mas)	m (% in EVN)	σ_m (%)	EVPA ($^\circ$)	σ_{EVPA} ($^\circ$)
<i>J0724 + 4159</i>	(-129, 228)	(-150, 210)	11	3.9	113.8	11.6
<i>J0728 + 4026</i>	(-126, 224)	(-120, 210)	4.7	1.5	131.9	34.7
<i>J1044 + 3656</i>	(225, -225)	(210, -240)	3.2	1.3	125.9	32.9
<i>J1122 + 3124</i>	(-123, -200)	(-120, -210)	3.0	1.3	81.9	7.7
<i>J1150 + 2819</i>	(45, -58)	(30, -60)	3.1	1.3	5.8	30.0
<i>J1413 + 4212</i>	(-158, -5)	(-180, 0)	3.3	1.3	85.5	32.9
<i>J1603 + 3002</i>	(-104, -171)	(-120, -180)	1.3	0.3	126.4	34.7
<i>J1655 + 3945</i>	(18, -66)	(30, -60)	4.1	1.4	49.2	26.6

Column(1): IAU name in J2000; Column(2): distance from EVN phase tracking center; Column(3): distance from MERLIN phase tracking center; Column(4): percentage polarization in EVN observations; Column(5): uncertainty for percentage polarization in EVN observations; Column(6): EVPA in EVN observations; Column(7): uncertainty for EVPA.

Table 3. The VLBI positions of 11 BAL quasars, including 3 previously observed BAL quasars.

Source	RA (hh mm) (J2000)	Dec (dd mm) (J2000)	reference	reference RA (J2000)	reference Dec (J2000)	RA (hh mm) (J2000)	Dec (dd mm) (J2000)
<i>J0724 + 4159</i>	07 24 18.4920	+41 59 14.400	<i>J0730 + 4049</i>	07 30 51.3466	+40 49 50.827	07 24 18.4834	+41 59 14.628
<i>J0728 + 4026</i>	07 28 31.6610	+40 26 15.850	<i>J0730 + 4049</i>	07 30 51.3466	+40 49 50.827	07 28 31.6526	+40 26 16.074
<i>J1044 + 3656</i>	10 44 59.5910	+36 56 05.390	<i>J1050 + 3430</i>	10 50 58.1230	+34 30 10.941	10 44 59.6060	+36 56 05.165
<i>J1122 + 3124</i>	11 22 20.4620	+31 24 41.200	<i>J1130 + 3031</i>	11 30 42.4292	+30 31 35.388	11 22 20.4538	+31 24 41.000
<i>J1150 + 2819</i>	11 50 23.5700	+28 19 07.500	<i>J1147 + 2635</i>	11 47 59.7639	+26 35 42.333	11 50 23.5730	+28 19 07.442
<i>J1413 + 4212</i>	14 13 34.4040	+42 12 01.760	<i>J1405 + 4056</i>	14 05 07.7954	+40 56 57.831	14 13 34.3935	+42 12 01.755
<i>J1603 + 3002</i>	16 03 54.1620	+30 02 08.880	<i>J1605 + 3001</i>	16 05 33.0480	+30 01 29.702	16 03 54.1551	+30 02 08.709
<i>J1655 + 3945</i>	16 55 43.2350	+39 45 19.940	<i>J1652 + 3902</i>	16 52 58.5096	+39 02 49.823	16 55 43.2362	+39 45 19.874
<i>J0957 + 2356*</i>	09 57 07.3670	+23 56 25.320	<i>J0956 + 2515</i>	09 56 49.8754	+25 15 16.050	09 57 07.3712	+23 56 25.379
<i>J1312 + 2319*</i>	13 12 13.5600	+23 19 58.510	<i>J1321 + 2216</i>	13 21 11.2014	+22 16 12.092	13 12 13.5753	+23 19 58.572
<i>J1556 + 3517*</i>	15 56 33.7720	+35 17 57.620	<i>J1602 + 3326</i>	16 02 07.2635	+33 26 53.072	15 56 33.7768	+35 17 57.389

Column(1): IAU name of BAL quasar in J2000, * denotes perviously observed source; Column(2): RA measured by VLA in J2000; Column(3): Dec measured by VLA in J2000; Column(4): IAU name of phase-reference source in J2000; Column(5): RA for phase-reference source; Column(6): Dec for phase-reference source; Column(7): RA remeasured for BAL quasar by our EVN observation in J2000; Column(8): Dec remeasured for BAL quasar by our EVN observation in J2000.

Table 4. Optical line information from SDSS released data and black hole mass for sources in our sample.

Sources Name	Redshift	$f_{\lambda 3000}$ (10^{-17} ergs $s^{-1} \text{\AA}^{-1} \text{cm}^{-2}$)	FWHM (km s^{-1})	lines	M_{BH} $10^8 M_\odot$
<i>J0724 + 4159</i>	1.551	85	2428	Mg II	0.26
<i>J1044 + 3656</i>	0.702	201	4197	H β	3.98
<i>J1122 + 3124</i>	1.453	124	2518	Mg II	0.34
<i>J1150 + 2819</i>	3.124	323	2069	C IV	0.59
<i>J1413 + 4212</i>	2.817	225	6116	C IV	4.47
<i>J1603 + 3002</i>	2.030	95	1619	Mg II	0.11
<i>J1655 + 3945</i>	1.753	80	1529	Mg II	0.09

Col. (1): Object name. Col. (2): Redshift. Col. (3): flux density at 3000\AA in units of 10^{-17} ergs $s^{-1} \text{\AA}^{-1} \text{cm}^{-2}$. Col. (4): full width at half maximum (FWHM) of broad line in units of km s^{-1} . (5): line used for FWHM. Col. (6): black hole mass in unit of $10^8 M_\odot$. See Kaspi et al. (2005) and McLure & Jarvis (2002) for the detailed method of the black hole mass calculation.

3 SOURCES AND RESULTS

3.1 J0724+4159

J0724+4159 is a LoBAL quasar. The radio source associated with this quasar is unresolved in the VLA observation at 20 cm. Its flux density is 7.9 mJy in FIRST. J0724+4159 has a spectral index between 20 cm and 3.6 cm of $\alpha = 0.0$. The radio loudness is $\log R = 1.6$ (Becker et al. 2000). The naturally weighted image with the EVN (Fig.1(a)) still shows an unresolved structure at 18 cm, with a total flux density of 7.2 mJy. With the same weighting, the image derived from MERLIN gives a total flux density of 8.0 mJy. Since the difference in the flux density between EVN and MERLIN is consistent with the uncertainty of the flux calibration, we believe that there are no missing components in J0724+4159 at high angular resolution with EVN. The compact component in the EVN image of J0724+4159 shows a high polarization level of $\sim 11\%$.

3.2 J0728+4026

J0728+4026 was discovered as a LoBAL quasar. It is a point source with 18 mJy with the VLA at 18 cm (A-configuration). The flux density with the VLA A-configuration at 3.6 cm is 2.7 mJy. These non-simultaneous data suggest a steep spectral index $\alpha = -1.1$. Its radio loudness is $\log R = 0.37$ (Becker et al. 2000). The naturally weighted image with the EVN (Fig.1(b)) shows a core-jet structure. The flux density in the core-jet structure is 16.1 mJy in EVN observation, which accounts for about 92% of the total flux density of 17.3 mJy detected by MERLIN. The core-jet structure has a degree of polarization of about 4.7%.

3.3 J1044+3656

J1044+3656 is a LoBAL quasar. The VLA observation in A-configuration at 20 cm suggests that this source is unresolved with a flux density of about 15.6 mJy. The spectral index between 20 cm and 3.6 cm is $\alpha = -0.5$. The radio loudness is $\log R = 1.29$ (Becker et al. 2000). The naturally weighted image with the EVN (Fig.1(c)) displays a core-jet structure at 18 cm with a total flux density of 16.4 mJy. MERLIN detected a flux density of about 18.5 mJy. There might be some weak structures resolved out in the EVN image. The difference in the flux density between the VLA and MERLIN images is probably due to source variation.

J1044+3656 shows a fractional polarization of about 3.2% in the central component. The two different directions of the electric vector in the compact region in the EVN map may

come from two different components, one being the core and another the jet component. The jet component might be only just separated from the core, its direction of electric vector following the jet direction.

3.4 J1122+3124

J1122+3124 is a LoBAL quasar. The spectral index between 20 cm and 3.6 cm obtained by the VLA in D-configuration is $\alpha = -0.6$. The estimated radio loudness is $\log R = 1.52$ (Becker et al. 2000). The naturally weighted image of the source with the EVN (Fig.1(d)) shows a central component with two-sided structure at 18 cm, which is nearly aligned with the central component. The southern component is located 150 mas away from the central component, while a weak northern component lies 87 mas away. About 90% of the flux density is present in the central component. In order to confirm the two-sided structure, we combined EVN and MERLIN data with different weights (see Fig.2). It seems that the northern component has more extended structure. The flux densities of the clean components in the EVN and MERLIN images are 8.3 mJy and 10.2 mJy, respectively. The extended northern emission was probably resolved at EVN resolution. The source may vary. The flux density measured by the VLA is 12.9 mJy in B-configuration at 20 cm, and another two measurements at the same frequency with the VLA are 10.9 mJy and 10.0 mJy in D-configuration (Becker et al. 2000).

The naturally weighted EVN image shows about 3.0% fractional polarization in the central component, but it is not detected in the two-sided lobes because of their weak intensity. The fractional polarization with MERLIN is about 2.7%, which is consistent with the EVN result.

3.5 J1150+2819

J1150+2819 is a HiBAL quasar. The VLA observation at 20 cm shows an unresolved image with a flux density of about 14.2 mJy. The spectral index between 20 cm and 3.6 cm is $\alpha = -1.2$. The estimated radio loudness is $\log R = 1.43$ (Becker et al. 2000). The naturally weighted image with the EVN (Fig.3(a)) still displays unresolved structure at 18 cm. The clean components sum to 12.6 mJy in the EVN measurement, and 12.3 mJy with MERLIN. J1150+2819 shows a fractional polarization of about 3.1% in the central component.

3.6 J1413+4212

J1413+4212 is a HiBAL quasar. It is a point source with 18.7 mJy in the FIRST catalog. The flux density measured with the VLA at 3.6 cm in the D-configuration is 11.3 mJy. This gives a flat spectral index $\alpha = -0.2$. The radio loudness is $\log R = 1.68$ (Becker et al. 2000). The naturally weighted image with the EVN (Fig.3(b)) displays a short core-jet structure at 18 cm with 17.1 mJy. The MERLIN array measures about 18.1 mJy in clean components. The central component has 3.3% fractional polarization.

3.7 J1603+3002

J1603+3002 is a HiBAL quasar. It is the most luminous source in these observations. It has a radio loudness $\log R = 2.04$ (Becker et al. 2000). The flux densities at 20 cm and 3.6 cm detected by the VLA in A-configuration are 54.2 mJy and 18.1 mJy respectively, which suggests a spectral index of $\alpha = -0.6$. The total flux density is about 52.1 mJy in the EVN image (see Fig.3(c)). The MERLIN image shows an unresolved structure with 52.6 mJy flux density. The fractional polarization of the EVN image is about 1.3%.

3.8 J1655+3945

J1655+3945 is a HiBAL quasar. The VLA observation at 20 cm shows an unresolved image. The flux density of J1655+3945 in the FIRST catalog is 10.2 mJy. The spectral index between 20 cm and 3.6 cm is $\alpha = -0.2$. Its radio loudness is $\log R = 1.41$ (Becker et al. 2000). The naturally weighted EVN image depicts a resolved structure elongated to the south west with a total of 12.1 mJy (Fig.3(d)). In the central component the fractional polarization is about 4.1%.

4 DISCUSSION

The origin of the radio emission from these radio intermediate quasars is not fully understood. Based on the high brightness temperature inferred from radio variability, Zhou et al. (2006) suggested that the emission comes from relativistic jets for a small sub-sample of radio-loud BAL QSOs, while Blundell & Kuncic (2007) argued that the emission is produced by free-free emission from outflows in radio-weak QSOs. The brightness temperature in the source rest frame for the strongest components of these BAL quasars, based on the results

of model-fitting, range from $2.0 \times 10^9 \text{K}$ to $5.2 \times 10^{10} \text{K}$. The high brightness temperature and moderate polarization degree suggest that the radio is synchrotron emission from the jet.

Including the two-sided structure source J1122+3124, all BAL quasars that we observed with EVN+MERLIN at 18 cm exhibit a compact structure with a projected size of less than 2 kpc. In addition to J1122+3124, the total flux densities of the other seven compact sources measured with EVN at 18 cm are very close to the flux densities measured by both our simultaneous MERLIN and previous VLA observations at 20 cm. Therefore, if there is any low brightness extended structure in these object, it must be weak. Assuming that the 3.6 cm radio emission of these BAL quasars measured with the VLA comes from the compact component and they are non-variable, their radio spectra can be calculated by using VLA measurements between 20 cm and 3.6 cm. Five are steep-spectrum radio sources, and the rest are flat-spectrum sources. Combined with our previous observations of another three compact BAL quasars (see § 1) (Jiang & Wang 2003), there are seven steep-spectrum BAL quasars and four flat-spectrum sources. In these 11 compact BAL quasars observed with the EVN (or EVN+MERLIN) array, there is no significant difference between HiBAL and LoBAL quasars in their radio morphology and polarization. Similarly, there is no apparent difference in radio properties between flat- and steep-spectrum BAL quasars.

Among the seven steep-spectrum sources, five (J0728+4026, J1044+3656, J1150+2819, J1603+3002 and J0957+2356) show only compact cores or core-jet structures. In these cases there is no good indicator for the symmetry axis of the system, and the inclination might be distributed over a large range of values. However, although their sizes are much smaller than the typical values for Compact Steep Spectrum (CSS) sources (~ 15 kpc), it is likely that these BAL quasars could be related to CSS sources (e.g. Kunert-Bajraszewska & Marecki 2006). The remaining two steep-spectrum sources, J1122+3124 and J1312+2319, exhibit two-sided structure. According to the unification scheme, the orientation of their jets are far from the line of sight. The sizes of the radio sources are less than 2 kpc, the same as the typical size of Compact Symmetric Object (CSO). However, their central components account for more than 80% of the total flux density, which is significantly different from the structure of CSOs or FR II quasars, which have weak cores at low frequencies in general. Given the weakness of the lobes in both objects at 18 cm, it is plausible that their cores also have steep spectra. Therefore, these two sources are similar to other steep-spectrum radio BAL quasars except for the detection of weak extended lobes. The compact, steep-spectrum central component in these two BAL quasars suggest a link to the CSS sources.

The four flat-spectrum sources, J0724+4159, J1413+4212, J1556+3517 and J1655+3945, show core-dominated or marginal core-jet structures in the EVN/MERLIN maps. There are two possible interpretations for this. If their compact component is relativistically beamed emission from the base of the jet, the jet in these BAL quasars is near the line of sight. Their flat spectra are consistent with this interpretation. The degree of polarization of a few to ten percent is also typical for such sources. On the other hand, the flat, compact core might be related to the GHz peaked sources (GPS) (e.g., Benn et al. 2005). Noting that with an $\alpha = 0$ between 3.6 cm and 20 cm for J0724+4159, the peak frequency is likely to be around a few GHz in the observer's rest frame. For the other three, with spectral indexes of $\alpha = 0.1$ and 0.2 between 3.6 cm and 20 cm, the turnover frequency is also likely to be in the GHz range although further observations are needed to confirm this.

Our results suggest that the simple unification of BAL and non-BAL quasars by orientation is problematic. All the BAL quasars in our sample have compact radio morphology, including two-sided structure sources. If these BAL quasars are intrinsically small sources with relativistic jets, they can be observed either pole-on and edge-on. This scenario is not consistent with the current popular disk-wind models. Basing on their radio spectrum and morphology, the steep-spectrum BAL quasars could be classified as CSS, while the flat-spectrum BAL quasars might be GPS sources (Becker et al. 2000; Gregg et al. 2000). Both CSS and GPS sources are generally thought to represent the early stage in quasar lifetimes (O'Dea 1998). Due to their low luminosity, these BAL quasars might be located at the low end of radio power. Meanwhile, as for those radio luminous BAL quasars, a significant anti-correlation between radio loudness and the strength of the BAL features is exhibited in a total of eleven FR II-BAL quasars (Gregg, Becker & Vries, 2006) so far. The rarity of the FR II-BAL quasars indicates that the period of FR-II type combined BAL feature is very short (Gregg et al. 2006). This suggests an evolutionary picture in which FR II-BAL sources are frustrated by the obscuring BAL shroud until the quasars can boil away enough of the material through radiation pressure. Meanwhile, comparing the black hole mass and accretion rate between two small samples of BAL and non-BAL quasars, Yuan & Wills (2003) suggests that BAL quasars have a more plentiful fuel supply than non-BAL quasars, which might be related to the young age of this kind of source. In addition, by using optical information from released SDSS data, we derived black hole masses for 7 BAL quasars in our sample within the range $9.3 \times 10^6 M_{\odot}$ to $4.5 \times 10^8 M_{\odot}$ (see detailed information in Table

4). Despite the limited numbers in the sample, the comparatively low black hole masses of these BAL quasars might also be connected to their stage in the evolutionary sequence.

5 CONCLUSIONS

We present the results of EVN plus MERLIN polarization observations of 8 BAL quasars at 1.6 GHz, including 4 LoBALs and 4 HiBALs with either steep or flat spectra on VLA scales. The main conclusions are summarized as follows:

- Only one steep-spectrum source, J1122+3124, shows two-sided structure on the scale of 2 kpc. The other four steep-spectrum sources and three flat-spectrum sources display either an unresolved image or a core-jet structure on scales of less than three hundred parsecs, well within the galaxy size. In all cases, the marginally resolved core is the dominant radio component. Making use of the phase-reference technique, celestial positions are derived from our observations which are more accurate than those from the VLA.
- Linear polarization has been detected in the core in the range of a few to 10 percent. Polarization, together with high brightness temperatures (from $2 \times 10^9 - 5 \times 10^{10}$ K), suggest a synchrotron origin for the radio emission. There is no apparent difference in the radio morphologies or polarization between low-ionization and high-ionization BAL quasars nor between flat- and steep-spectrum sources.
- We considered compact steep-spectrum or GHz peaked radio source at the low end of radio power as the most likely explanation for these radio BAL QSOs. Therefore, they are probably a population of young radio sources.

ACKNOWLEDGMENTS

We are grateful to I. W. A. Browne and X. W. Cao for helpful suggestions and discussions. We thank the anonymous referee for insightful comments and constructive suggestions. We also thank Richard Porcas for helpful proofreading that improved the presentation of this work. The work is supported by the NSFC under grants 10373019, 10333020. TW acknowledges financial support NSFC 10573015. The European VLBI Network is a joint facility of European, Chinese, and other radio astronomy institutes funded by their national research councils. MERLIN is operated as a National Facility by the University of Manchester at Jodrell Bank Observatory on behalf of the UK Particle Physics & Astronomy Research Council. This research has made use of the NASA/ IPAC Extragalactic Database (NED), which is

operated by the Jet Propulsion Laboratory, California Institute of Technology, under contract with the National Aeronautics and Space Administration. This paper has made use of data from the SDSS. Funding for the creation and the distribution of the SDSS Archive has been provided by the Alfred P. Sloan Foundation, the participating institutions, the National Aeronautics and Space Administration, the National Science Foundation, the US Department of Energy, the Japanese Monbukagakusho, and the Max Planck Society.

REFERENCES

- Becker, R. H., White, R. L., et al. 2000, ApJ, 538, 72B
- Benn, C. R., Carballo, R., Holt, J., et al. 2005, MNRAS, 360, 1455
- Blundell, K. M. & Kuncic, Z. 2007, ApJ, 668,103
- Boroson, T. A. & Meyers, K. A. 1992, ApJ, 397, 442
- Boroson, T. A. 2002, ApJ, 565, 78
- Briggs, F. H., Turnshek, D. A., & Wolfe, A. M. 1984, ApJ, 287, 549
- Brotherton, M. S., Croom, S. M., De Breuck, C., et al. 2002, AJ, 124, 2575
- Cohen, M. H., Ogle, P. M., et al. 1995, ApJ, 448, L77
- Ghosh, K. K. & Punsly, B. 2007, ApJ, 661, 139
- Gregg, M. D., Becker, R. H., et al. 2000, ApJ, 544, 142
- Gregg, M. D., Becker, R. H., & Vries, W. D., 2006, ApJ, 641, 210
- Goodrich, R. W., & Miller, B. J., 1995, ApJ, 448, L73
- Hewett, P. C. & Foltz, C. B., 2003, AJ, 125, 1784
- Hines, D. H., & Wills, B. J., 1995, ApJ, 448, L69
- Jarvis, M. J. & McLure, R. J. 2002, MNRAS, 336, L38
- Jiang, D. R., Wang, T. G., 2003, A&A, 397, L13
- Kaspi, S., Maoz, D., Netzer, H. et al. 2005, ApJ, 629, 61
- Kunert-Bajraszewska, M. & Marecki, A. astro-ph/0612490v1
- Menou, K., Vanden Berk D. E., et al. 2001, ApJ, 561, 645
- O’Dea, C. P., 1998, PASP, 110, 493
- Punsly, B., 2006, ApJ, 647, 886
- Reichard, T. A., et al. 2003, AJ, 125, 1711
- Shen, Y., Strauss, M. A., Hall, P. B. et al. 2008, ApJ, 677, 858
- Shepherd, M. C., Pearson, T. J. & Taylor, G. B. 1994, BAAS, 26, 987

- Tolea, A., Krolik, J. H., & Tsvetanov, Z., 2002, *ApJ*, 578, L31
- Urry, C. M. & Padovani, P. 1995, *PASP*, 107, 803
- Wang, H. Y., Wang, T. G. & Wang, J. X. 2005, *ApJ*, 634, 149
- Weymann, R. J., Morris, S. L., et al. 1991, *ApJ*, 373, 23
- Weymann, R. J., 2002, in *Mass outflow in Active Galactic Nuclei: New Perspective*, ed. D. M. Crenshaw, S. B. Kraemer, & I. M. George (San Francisco: ASP), 329
- Willott, C. J., Rawlings, S., Grimes, J. A., 2003, *ApJ*, 598, 909
- Wills, B. J., Brandt, W. N. & Loar, A., 1999, *ApJ*, 520, L91
- Yuan, M. J. & Wills, B. J., 2003, *ApJL*, 593, 11Y
- Zhou, H. Y., Wang, T. G., Wang, H. Y. et al. 2006, *ApJ*, 639, 716

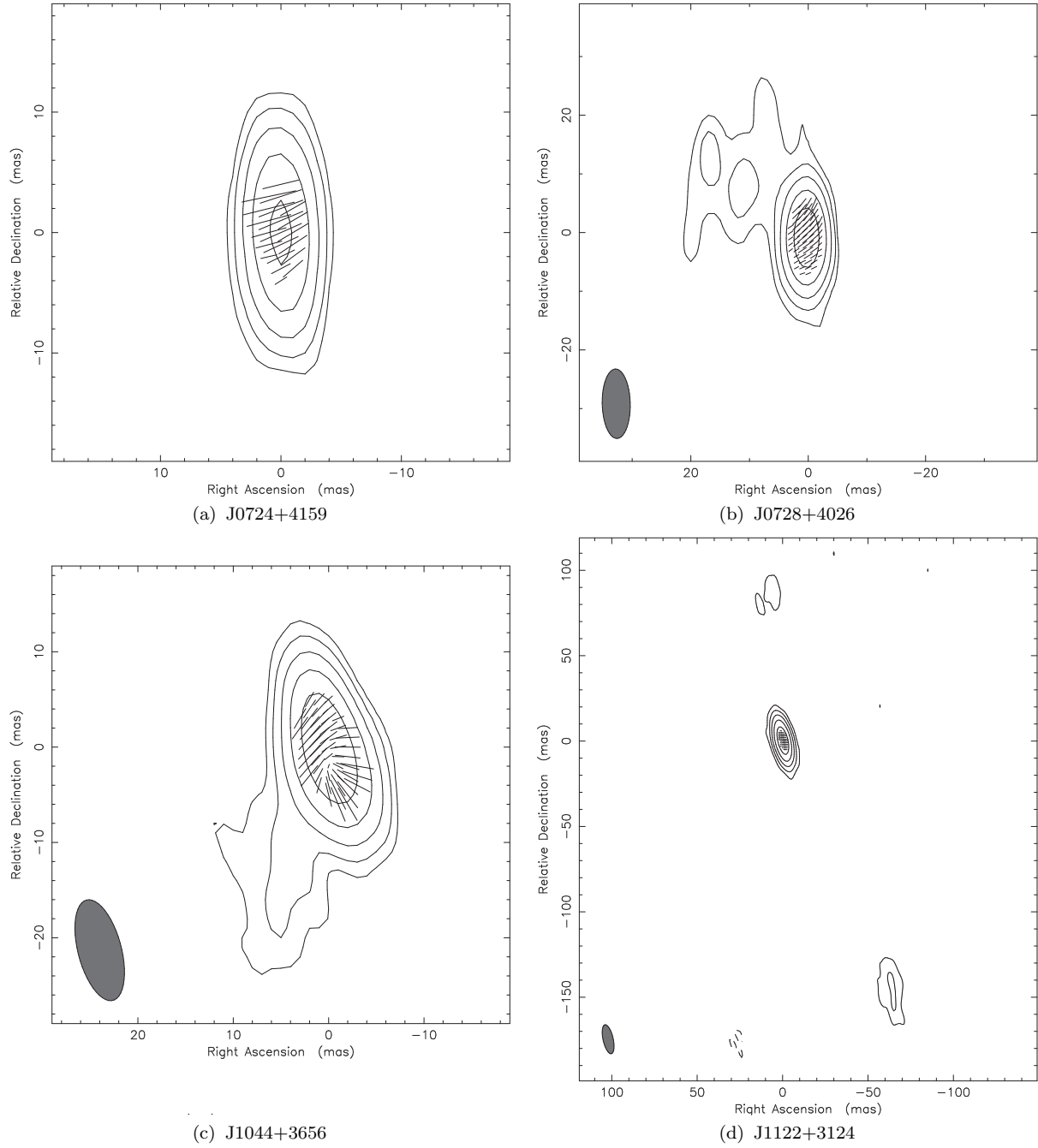


Figure 1. EVN images of LoBAL quasars at 1.6 GHz. (a): The restoring beam is 12.2×4.3 mas at $\text{P.A.} = 3.3^\circ$, the contour levels are $(1, 2, 4, 8, 16) \times 0.383$ mJy/beam, and the peak flux density is 7.0 mJy/beam. (b): The restoring beam is 11.8×4.8 mas at $\text{P.A.} = 1.3^\circ$, the contour levels are $(1, 2, 4, 8, 16) \times 0.443$ mJy/beam, and the peak flux density is 11.2 mJy/beam. (c): The restoring beam is 10.9×4.6 mas at $\text{P.A.} = 14.8^\circ$, the contour levels are $(1, 2, 4, 8, 16) \times 0.343$ mJy/beam, and the peak flux density is 10.8 mJy/beam. (d): The restoring beam is 17.4×5.9 mas at $\text{P.A.} = 12.6^\circ$, the contour levels are $(-1, 1, 2, 4, 8, 16) \times 0.240$ mJy/beam, and the peak flux density is 6.71 mJy/beam.

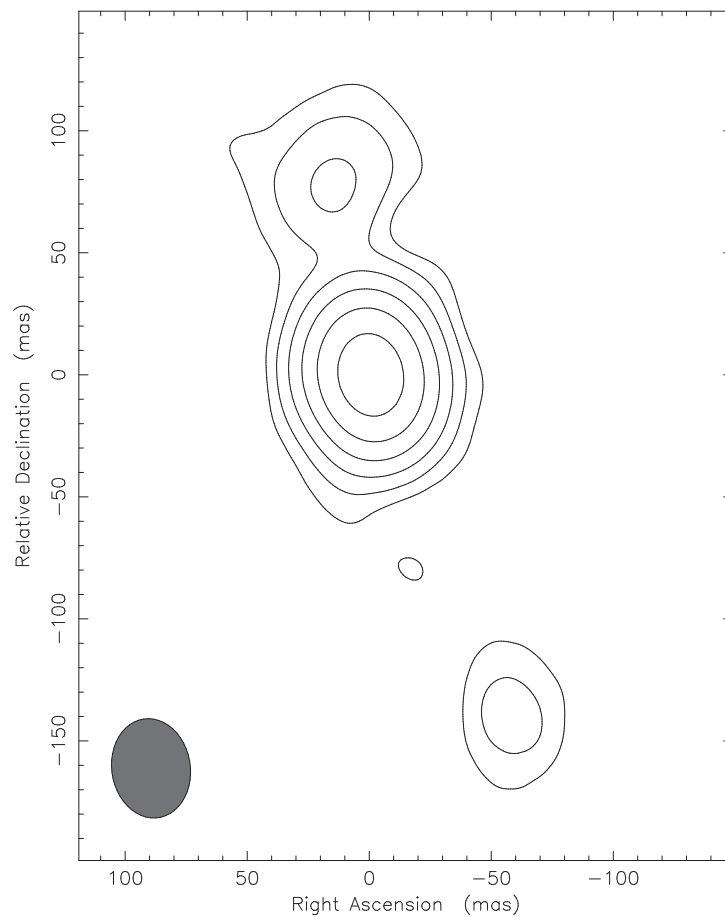


Figure 2. EVN+MERLIN combined image of BAL quasar J1122+3124 at 1.6 GHz. The restoring beam is 40.9×32.2 mas at P.A. = 8.5° . The contour levels are $(1, 2, 4, 8, 16, 32) \times 0.167$ mJy/beam. The peak flux density is 8.29 mJy/beam.

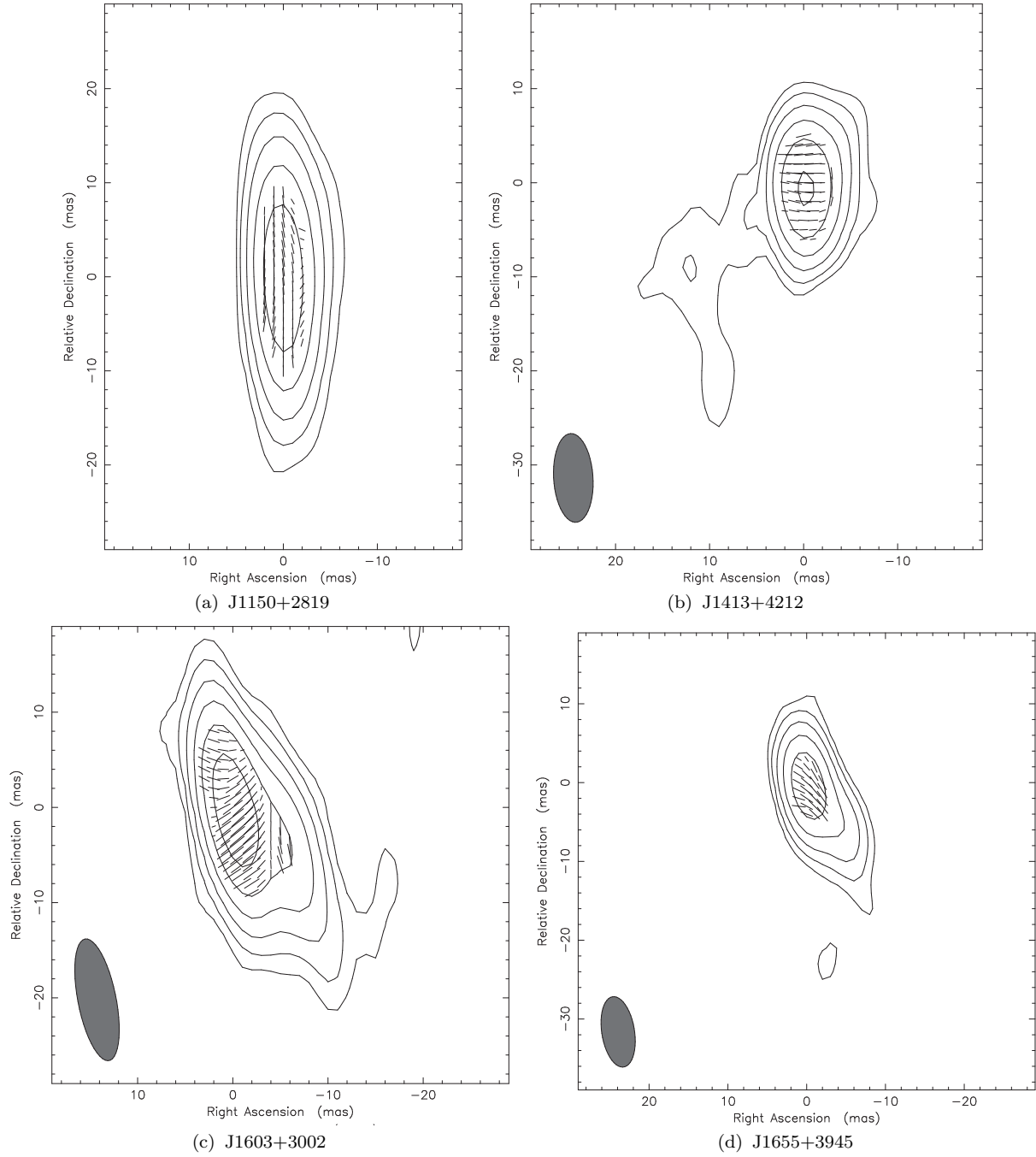


Figure 3. EVN images of HiBAL quasars at 1.6 GHz. (a): The restoring beam is 18.1×4.4 mas at $\text{P.A.} = 2.5^\circ$, the contour levels are $(1, 2, 4, 8, 16) \times 0.432$ mJy/beam, and the peak flux density is 11.7 mJy/beam. (b): The restoring beam is 9.5×4.2 mas at $\text{P.A.} = 3.6^\circ$, the contour levels are $(1, 2, 4, 8, 16, 32) \times 0.362$ mJy/beam, and the peak flux density is 12.7 mJy/beam. (c): The restoring beam is 13.0×4.0 mas at $\text{P.A.} = 11.2^\circ$, the contour levels are $(1, 2, 4, 8, 16, 32) \times 0.669$ mJy/beam, and the peak flux density is 37.1 mJy/beam. (d): The restoring beam is 9.0×4.2 mas at $\text{P.A.} = 9.1^\circ$, the contour levels are $(1, 2, 4, 8, 16) \times 0.313$ mJy/beam, and the peak flux density is 8.84 mJy/beam.